








## ORIGINAL ARTICLE

# Dynamic optical coherence tomography for imaging acute wound healing

Sandra Schuh<sup>1</sup>  | Maximilian Berger<sup>1</sup>  | Stefan Schiele<sup>2</sup>  |  
 Anna Rubeck<sup>2</sup>  | Gernot Müller<sup>2</sup> | Jennifer Jahel Vélez González<sup>1</sup>  |  
 Jon Holmes<sup>3</sup>  | Julia Welzel<sup>1</sup> 

<sup>1</sup>Department of Dermatology and Allergology, University Hospital Augsburg, Augsburg, Germany

<sup>2</sup>Institute of Mathematics, University of Augsburg, Augsburg, Germany

<sup>3</sup>Michelson Diagnostics Ltd, Maidstone, UK

## Correspondence

Sandra Schuh, Department of Dermatology and Allergology, University Hospital Augsburg, Sauerbruchstr. 6, 86179 Augsburg, Germany.  
 Email: [sandra.schuh@uk-augsburg.de](mailto:sandra.schuh@uk-augsburg.de)

## Funding information

European Union's ICT Policy Support Program as part of the Competitiveness and Innovation Framework Program, Grant/Award Number: 621015

## Abstract

The aim of this study was to investigate acute wound healing with dynamic optical coherence tomography (D-OCT). From 22 patients with 23 split skin graft donor sites, vessels at four wound edges, the wound bed, and adjacent and unaffected skin of the contralateral leg were measured by D-OCT at six time points from surgery to 4 weeks of healing. Changes in vessel orientation, density, diameter, morphology and pattern in horizontal, vertical and 3D images were analysed for wound healing and re-epithelialization. At 300 µm depth, there were significant differences of blobs and serpiginous vessels between normal and wounded skin. The wound had significantly more vertically oriented vessels, a higher degree of branching, vessel density and diameter compared with healthy skin. 3D images showed increased angiogenesis from healthy skin towards the wound centre, significantly higher vessel density at the wound than at normal skin and the highest at the interface. During wound healing blobs, coils and serpiginous vessels occurred significantly more frequently in lesional than healthy skin. Vessel density was greatest at the beginning, decreased and then increased by 4 weeks post-surgery. D-OCT helps to evaluate acute wound healing by visualizing and quantifying blood vessel growth in addition to re-epithelialization.

## KEYWORDS

acute wounds, angiogenesis, optical coherence tomography, re-epithelialization, wound healing

## Key Messages

- D-OCT helps to evaluate acute wound healing by visualizing blood vessel growth.
- The aim of the study was to investigate acute wound healing with D-OCT.

This is an open access article under the terms of the [Creative Commons Attribution-NonCommercial-NoDerivs](https://creativecommons.org/licenses/by-nc-nd/4.0/) License, which permits use and distribution in any medium, provided the original work is properly cited, the use is non-commercial and no modifications or adaptations are made.

© 2024 The Author(s). *International Wound Journal* published by Medicalhelplines.com Inc and John Wiley & Sons Ltd.

- The vessel shapes blobs, coils and serpiginous vessels were significantly more common in the wound area than in unaffected healthy skin during wound healing.
- Vessel density was high at the beginning of wound healing, decreased and then increased again at the end of 4 weeks of follow-up.

## 1 | INTRODUCTION

Acute wounds generally heal faster than chronic wounds. Good blood and oxygen supply are the most important components for successful wound healing. Therefore, the study of blood vessels is essential for understanding the wound healing process. At the beginning of wound healing, haemostasis plays a major role, and over time, the transport of metabolites leads to the nutrition and immune defence of wound tissue.<sup>1</sup>

Split-thickness skin grafts have a thickness of about 0.4 mm. Thus, they cause defects of the epidermis and upper dermis, leading to an abrasion of superficial skin layers.<sup>1,2</sup> Deeper skin levels are not affected. Therefore, the deep dermal blood plexus remains intact and may rebuild the superficial plexus to supply the newly formed epidermis. Surgical transection of the capillaries in the papillary layer removes the upper blood plexus, resulting in superficial punctate bleeding in the wound.

The injured tissue requires optimal neovascularization for rapid wound healing. Therefore, the study of the vascular system using dynamic optical coherence tomography (D-OCT) could be helpful in analysing pathophysiological processes that might prevent acute wounds from turning into severe scars or chronic wounds.<sup>3–5</sup>

Software-based devices for blood flow detection have been developed since 2015 and are referred to as speckle-variance OCT,<sup>6</sup> decorrelation-mapping OCT<sup>7</sup> and optical microangiography.<sup>8</sup> These methods are collectively known as OCT-angiography or D-OCT. D-OCT is superior to Doppler-OCT due to its lack of sensitivity caused by high noise and to Doppler flowmetry due of its lower resolution and lack of depth discrimination.<sup>9,10</sup> D-OCT is similar to laser speckle contrast imaging but offers the possibility to resolve depth below skin and visualize individual small blood vessels.<sup>11</sup> The ability to image blood capillaries in high resolution with depth measurement is why D-OCT could be a useful new tool for assessing vascular development in acute wounds non-invasively, painlessly, in real time and in vivo. Therefore, D-OCT can help to select appropriate therapies, monitor healing and treatment effects, and detect disturbances in wound healing, such as infections, at an earlier stage.

## 2 | MATERIALS AND METHODS

### 2.1 | Patients and procedure

Twenty-two patients (8 female, 15 male, median age 80.0 years, first quartile: 71 years, third quartile: 86 years, all non-smokers) with 23 split-thickness skin grafts (one patient received two skin grafts on the same thigh) participated in the study. Thirteen skin graft sites were on the right thigh, and 10 skin graft sites were on the left thigh. The median size of the grafts was 25 cm<sup>2</sup> (range 6.25 cm<sup>2</sup>–176 cm<sup>2</sup>). Each patient had an excised skin tumour and required a skin graft to cover the wound, which could not be closed by other means. The ethics committee of the Ludwig-Maximilian-University Munich (No. P30-14) and the ethics vote of the University of Lübeck, Germany (No. 97-061) approved the study. The study was conducted at the Department of Dermatology, University Hospital Augsburg, Germany. The principles of the Declaration of Helsinki and the international guidelines for human studies were always observed. The patients in this manuscript gave written informed consent for the publication of their case details.

Patients older than 18 years, with written signed informed consent, healthy skin at the donor site and adjacent areas, and unaffected perilesional skin as a control site were included. Patients with local and systemic infections, generalized skin diseases, systemic drugs (e.g., cytostatics or corticosteroids), allergies to topical treatments, scars, acute or chronic wounds, medications, or skin irritation in the scan area were excluded. Anticoagulants were allowed. Skin graft removal was performed by a dermatologist. The graft thickness was adjusted with the dermatome to 0.4 mm. The wound was measured and photographed with a Panasonic Lumix DMC-TZ8 camera. All patients received standardized treatment according to local protocol (Opsite<sup>®</sup> wound dressing 10 × 14 cm, followed by Allevyn<sup>®</sup> gentle border after 6 days). The wound was scanned with the D-OCT at the four wound edges (top, right, bottom and left) (Figure 1A). The fifth scan point was at the wound bed, the sixth scan point was at 2 cm outside the wound from unaffected skin and the seventh scan point was at the same location on the contralateral leg as a control. For each scan of the margin, the probe was oriented so that

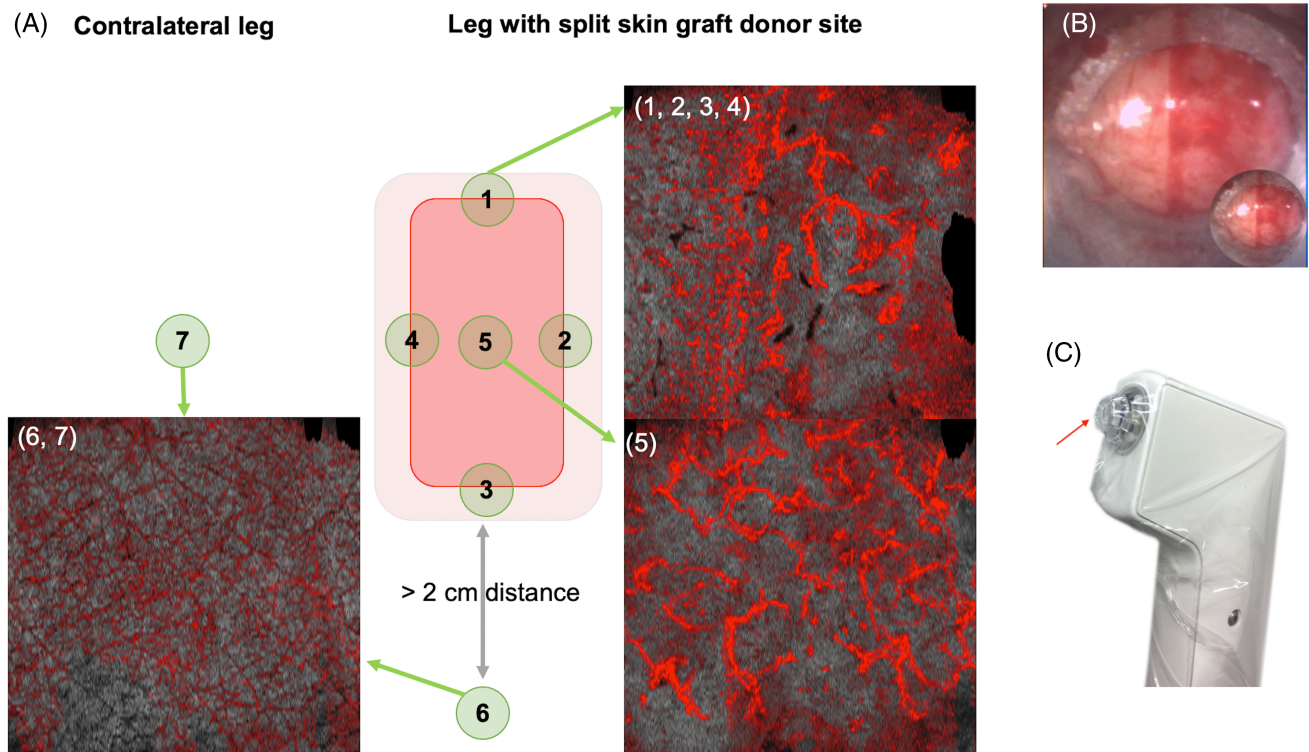


**FIGURE 1** Overview of the measurement process at the seven measurement points; position of the OCT probe in sterile sheath with spacer. (A) Illustrates the standardized measurement process at seven different measurement points, which were scanned at every patient's visit. Scans were conducted at the midpoint of the four wound edges (1–4), at the wound bed (5), at least 2 cm adjacent to the wound (6) and at the same location on the contralateral leg (7). The corresponding D-OCT images illustrate the branching, diameter and density of vessels depending on the measurement point (1 = wound edge, 5 = wound bed, 6, 7 = normal skin). Compared with normal skin (6, 7), more arborizing vessels were found at the wound edge or bed (1–5). In healthy skin, vessels with a smaller diameter appeared (6, 7). At the wound edge (1–4), smaller vessels were more common than in the wound bed (5). In normal skin, vessel density was nearly absent or very low (6, 7), whereas vessel density at the wound edge or bed was of medium size (1–5). (B) shows the standardized scanning position of the probe with healthy skin on the left side of the image and the wound on the right side. (C) Depicts the OCT probe enclosed in sterile sheath, over which a sterilized 'standoff' (arrow) is fitted to set skin at the correct focal distance.

healthy skin was on the left side of the image and the wound was on the right side (Figure 1B). The protocol included six appointments for each patient over a 4-week period. Scans were taken on the day of surgery (day 0), and on Days 1, 4, 7, 14 and 28 after surgery.

## 2.2 | Dynamic optical coherence tomography

In this study, the VivoSight<sup>®</sup> Dx OCT scanner (Michelson Diagnostics Ltd, Maidstone, Kent, UK) was used with dynamic OCT imaging software. It is CE-marked and FDA 510(k) cleared for non-invasive in vivo skin imaging. Its use in open wounds is contraindicated due to the potential risk of cross-infection from a detachable plastic spacer used to keep the probe at the correct focal distance, which contacts the wound during scanning. For this study, pre-sterilized disposable spacers in sealed bags with approval from the ethics committee

were used. After each visit, a new set of spacers was opened, and the device was disinfected by wiping. A transparent sterile disposable sheath was placed over the OCT probe and cable (Figure 1C).

The OCT uses a laser wavelength of 1305 nm with an optical resolution of 7.5  $\mu\text{m}$  in the lateral and 5  $\mu\text{m}$  in the axial direction. The field of view is  $6 \times 6 \text{ mm}^2$  with a 1.0–2.0 mm depth. The D-OCT works well until 0.5 mm, but at greater depths, the image appears blurry due to background noise. The handpiece is equipped with a colour camera to help guide positioning and monitor the lesion. No gel or oil is used. The device acquires a 3D scan ( $6 \times 6 \times 2 \text{ mm}^3$ ) of 120 D-OCT images with a pixel size of 4.4  $\mu\text{m}$  in 30 s.

## 2.3 | D-OCT image analysis

ImageJ<sup>®</sup> was used to evaluate vessel morphology without adjustment or enhancement.<sup>3,12</sup> As in other D-OCT studies,<sup>5,14,15</sup> vessel morphology was assessed after

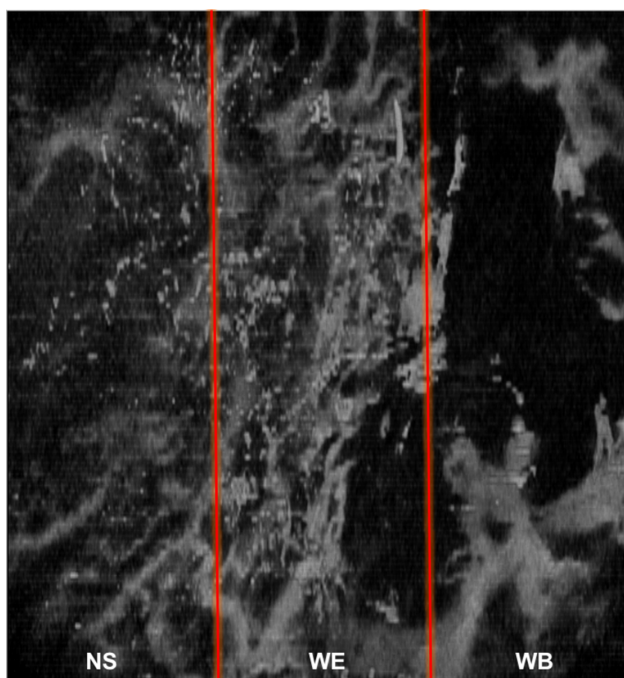


**FIGURE 2** Example of processing and trisection of an image for vessel density analysis. This figure shows the processed OCT image (6 mm × 6 mm) transitioning from healthy skin over the wound edge to the wound bed. The original OCT image in TIFF format displayed a red overlay of the vessels, which was converted to an 8-bit file, with brightness adjusted to 85 to reduce image noise. The processed image was analysed using Volume Viewer with the “measure” tool to calculate the density. This calculation was performed for the entire image and for three equal sections highlighted by red lines to visualize the healthy skin (NS), the wound edge (WE) and the wound bed (WB) from left to right. The density was shown as a percentage of tissue volume by measuring the average pixel intensity.

adjusting the surface to a flat line (“fitting”) at 150, 300 and 500  $\mu\text{m}$ . Vessel shapes were analysed in en face images regarding density, diameter, distribution (regular, irregular or clustered) and direction (no orientation, streaming or radiating) compared with healthy adjacent skin (less, average or more) according to Ulrich et al.<sup>13</sup> Vessel shapes were described using the terms dots (small points), blobs (larger points), coils (small, knotted vessels), clumps (large knot-like vessels), lines, curves and serpiginous vessels. Each shape was rated 0 = absent or 1 = present (S1). Vessel density was measured using ImageJ<sup>®</sup> 3D plugin Volume Viewer. The TIFF image was converted into an 8-bit file and brightness was uniformly corrected to the value of 85 to suppress the so-called image noise. The processed image was examined with Volume Viewer and the “Measure” tool by calculating the density of the entire image and of three equally sized image sections (for wound bed, wound edge and healthy skin) as a percentage (%) of tissue volume, which outputs

the average pixel intensity in the view (Figure 2). For vessel morphology and density, the average of the results from the scans of the four edges was calculated. The average of scan points six and seven was calculated for healthy skin.

## 2.4 | Statistics

Data were collected with Microsoft<sup>®</sup> Excel<sup>®</sup> for Windows 2016, and statistical analyses were performed with IBM<sup>®</sup> SPSS<sup>®</sup> Statistics Software for Windows (SPSS 24.0, IBM Corp., Armonk, NY, USA). Statistical analysis comparing the wound centre, wound border, and adjacent and contralateral skin was performed using the Wilcoxon matched pairs test. A  $p$ -value <0.05 was considered statistically significant.

## 3 | RESULTS

### 3.1 | Vascular shapes, vessel density and diameter in the en face view depending on the measurement location

Different vessel shapes were examined at three locations at 150, 300 and 500  $\mu\text{m}$  depth (Table 1). At 150  $\mu\text{m}$ , dots were always visible at each measurement point. The proportion of curves, blobs and lines was significantly different for wound edge (WE) and wound bed (WB) compared with normal skin on the contralateral leg (NSCL). All three vessel shapes were frequently present in WE and WB (curves: 68%/67%; blobs: 40%/51%; lines: 50%/46%) but less frequently in NSCL (curves: 30%; blobs: 7%; lines: 24%). Coils and serpiginous vessels were uncommon at all sites and only serpiginous vessels differed significantly between the measurement point locations.

At 300  $\mu\text{m}$ , dots, blobs, lines, curves and serpiginous vessels were observed in most cases. Coils were detected in approximately 20% of all wounds. All vessel shapes were present in a higher proportion of cases than at 150  $\mu\text{m}$ . Blobs and serpiginous vessels were frequently more present in both WE and WB compared with NSCL (blobs: 96%/ 96% vs. 77%; serpiginous: 85%/90% vs. 43%; all  $p < 0.001$ ). WE had a higher proportion of coils than NSCL (23% vs. 13%;  $p < 0.001$ ).

The results at 500  $\mu\text{m}$  depth were similar to those at 300  $\mu\text{m}$  depth. All vessel shapes except coils and serpiginous vessels were present in almost all cases. Coils and serpiginous vessels appeared in significantly higher proportions in WE and WB compared with NSCL (coils: 71%/ 80% vs. 49%; serpiginous vessels: 97%/98% vs. 77%; all  $p < 0.001$ ).

**TABLE 1** Prevalence in % of vessel shapes at 150, 300 and 500  $\mu\text{m}$  in en face view from all patients, observed at the wound edge (WE), wound bed (WB), normal skin 2 cm adjacent to the wound and unaffected skin from the contralateral leg (NSCL) across all time points.

150 $\mu\text{m}$	Dot		Blob		Coil		Line		Curved		Serpiginous	
	M $\pm$ SD	p-value	M $\pm$ SD	p-value	M $\pm$ SD	p-value	M $\pm$ SD	p-value	M $\pm$ SD	p-value	M $\pm$ SD	p-value
WE	100% $\pm$ 0%	1	40% $\pm$ 49.1%	0.637	5% $\pm$ 20.8%	0.637	50% $\pm$ 50.8%	0.904	68% $\pm$ 46.9%	0.674	26% $\pm$ 43.9%	0.005
WB	100% $\pm$ 0%		51% $\pm$ 50.2%		6% $\pm$ 23.5%		46% $\pm$ 50.1%		67 $\pm$ 47.0%		36% $\pm$ 48.0%	
WE	100% $\pm$ 0%	0.317	40% $\pm$ 49.1%	<0.001	5% $\pm$ 20.8%	0.074	50% $\pm$ 50.8%	<0.001	68% $\pm$ 46.9%	<0.001	26% $\pm$ 43.9%	<0.001
NSCL	100% $\pm$ 6.0%		7% $\pm$ 24.7%		2% $\pm$ 14.6%		24% $\pm$ 42.5%		30% $\pm$ 46.7%		1% $\pm$ 10.4%	
WB	100% $\pm$ 0%	1	51% $\pm$ 50.2%	<0.001	6% $\pm$ 23.5%	0.206	46% $\pm$ 50.1%	0.006	67 $\pm$ 47.0%	<0.001	36% $\pm$ 48.0%	<0.001
NSCL	100% $\pm$ 6.0%		7% $\pm$ 24.7%		2% $\pm$ 14.6%		24% $\pm$ 42.5%		30% $\pm$ 46.7%		1% $\pm$ 10.4%	
300 $\mu\text{m}$	Dot		Blob		Coil		Line		Curved		Serpiginous	
	M $\pm$ SD	p-value	M $\pm$ SD	p-value	M $\pm$ SD	p-value	M $\pm$ SD	p-value	M $\pm$ SD	p-value	M $\pm$ SD	p-value
WE	100% $\pm$ 0%	1	96% $\pm$ 19.7%	0.197	23% $\pm$ 42.2%	0.080	96% $\pm$ 20.4%	0.194	98% $\pm$ 14.6%	1000	85% $\pm$ 36.1%	0.513
WB	100% $\pm$ 0%		96% $\pm$ 20.5%		21% $\pm$ 40.9%		87% $\pm$ 33.8%		96% $\pm$ 18.8%		90% $\pm$ 30.3%	
WE	100% $\pm$ 0%	1	96% $\pm$ 19.7%	<0.001	23% $\pm$ 42.2%	0.001	96% $\pm$ 20.4%	0.493	98% $\pm$ 14.6%	0.074	85% $\pm$ 36.1%	<0.001
NSCL	100% $\pm$ 0%		77% $\pm$ 42.3%		13% $\pm$ 33.3%		93% $\pm$ 25.4%		95% $\pm$ 22.7%		43% $\pm$ 49.6%	
WB	100% $\pm$ 0%	1	96% $\pm$ 20.5%	<0.001	21% $\pm$ 40.9%	0.064	87% $\pm$ 33.8%	0.178	96% $\pm$ 18.8%	0.071	90% $\pm$ 30.3%	<0.001
NSCL	100% $\pm$ 0%		77% $\pm$ 42.3%		13% $\pm$ 33.3%		93% $\pm$ 25.4%		95% $\pm$ 22.7%		43% $\pm$ 49.6%	
500 $\mu\text{m}$	Dot		Blob		Coil		Line		Curved		Serpiginous	
	M $\pm$ SD	p-value	M $\pm$ SD	p-value	M $\pm$ SD	p-value	M $\pm$ SD	p-value	M $\pm$ SD	p-value	M $\pm$ SD	p-value
WE	100% $\pm$ 0%	1	98% $\pm$ 13.3%	0.102	71% $\pm$ 45.6%	0.033	99% $\pm$ 7.4%	0.157	100% $\pm$ 4.3%	1000	97% $\pm$ 17.8%	1
WB	100% $\pm$ 0%		99% $\pm$ 8.5%		80% $\pm$ 40.4%		100% $\pm$ 0%		100% $\pm$ 0%		98% $\pm$ 14.6%	
WE	100% $\pm$ 0%	1	98% $\pm$ 13.3%	0.405	71% $\pm$ 45.6%	<0.001	99% $\pm$ 7.4%	0.157	100% $\pm$ 4.3%	0.317	97% $\pm$ 17.8%	<0.001
NSCL	100% $\pm$ 0%		97% $\pm$ 17.8%		49% $\pm$ 50.1%		100% $\pm$ 0%		100% $\pm$ 6.0%		77% $\pm$ 42.3%	
WB	100% $\pm$ 0%	1	99% $\pm$ 8.5%	0.034	80% $\pm$ 40.4%	<0.001	100% $\pm$ 0%	1	100% $\pm$ 0%	0.317	98% $\pm$ 14.6%	<0.001
NSCL	100% $\pm$ 0%		97% $\pm$ 17.8%		49% $\pm$ 50.1%		100% $\pm$ 0%		100% $\pm$ 6.0%		77% $\pm$ 42.3%	

Note: A *p*-value < 0.05 was considered statistically significant. To emphasise these *p*-values, they have been written in bold letters.

Abbreviations: M, mean value; SD, standard deviation.

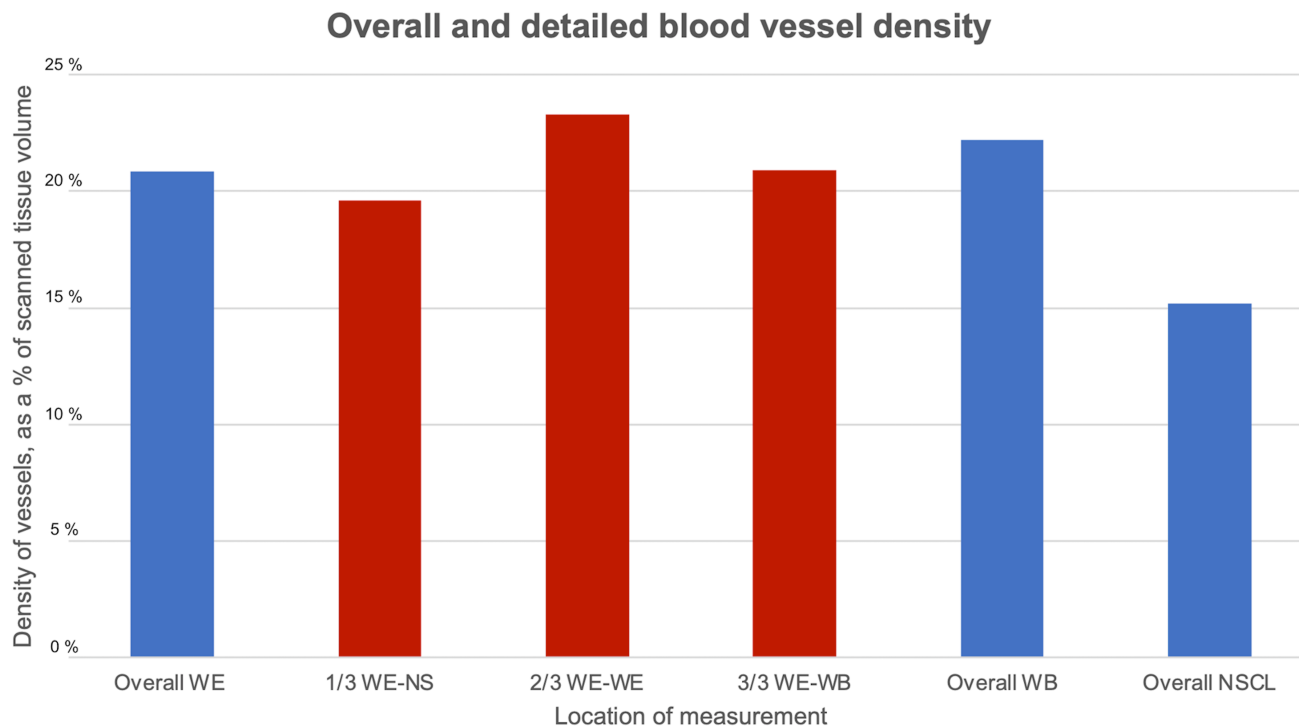


**FIGURE 3** Overall vessel densities measured at the wound edge (WE), wound bed (WB), normal skin 2 cm adjacent to the wound, and unaffected skin from the contralateral leg (NSCL) and the detailed vessel densities measured at three sections of one image at all averaged measurement time points. The measured vessel density varied from 14% to 22% of the total scanned tissue volume. The vessel density of NS was significantly lower compared with the wound (NSCL: 15.2% vs. WE: 20.9% and WB: 22.2%) (for each  $p < 0.001$ ). WB showed a significantly higher vessel density compared with WE ( $p < 0.001$ ). Overall vessel density for WE consisted of the averaged vessel densities of the wound edge locations 1–4. Overall vessel density for NSCL consisted of the averaged vessel densities of NS (normal skin 2 cm adjacent to the wounds) and of NSCL (unaffected skin from the contralateral leg). For overall density, the mean vessel density as a percentage of vessels within the whole image (6 mm x 6 mm) was calculated. For detailed density, the mean vessel density as a percentage of vessels within one third of the whole image (6 mm x 6 mm) was calculated. The whole image was divided into three parts (area of the WE-WE, WE-WB and WE-NS). The detailed vessel density varied from 15% to 23%. The vessel density was highest for 2/3 WE-WE (23.3%), followed by 3/3 WE-WB (20.9%) and 1/3 WE-NS (19.6%). The differences between each of the three thirds were significant ( $p < 0.001$ ).

**TABLE 2** Prevalence in % of vessel shapes in vertical view from all patients at the wound edge (WE), wound bed (WB), normal skin 2 cm adjacent to the wound and unaffected skin from the contralateral leg (NSCL).

	Spikes		Columns	
	MW ± SD	p-value	MW ± SD	p-value
WE	100% ± 4.3%	1	94% ± 23.7%	<b>0.012</b>
WB	100% ± 0%		98% ± 14.6%	
WE	100% ± 4.3%	<b>&lt;0.001</b>	94% ± 23.7%	<b>&lt;0.001</b>
NSCL	66% ± 47.6%		32% ± 46.5%	
WB	100% ± 0%	<b>&lt;0.001</b>	98% ± 14.6%	<b>&lt;0.001</b>
NSCL	66% ± 47.6%		32% ± 46.5%	

Note: The vessel shapes were counted as follows: 0 = absent, 1 = present. A  $p$ -value  $< 0.05$  was considered statistically significant. To emphasise these  $p$ -values, they have been written in bold letters.

Abbreviations: M, mean value; SD, standard deviation.

The rule for all vascular shapes is as follows: if a morphological structure appears, regardless of depth, it is generally more common in the wound than in healthy skin, provided that this shape does not occur with maximum frequency in healthy skin (such as dots). The mean frequency of the vessel shapes directly correlates with depth: the deeper the skin, the more frequently a vessel structure appears, regardless of the measuring area (based on a comparison of the frequency of vessel shapes at 150–500  $\mu$ m in Table 1 and Figure 4).

Normal skin exhibited either no or very low density of small-diameter vessels, whereas these vessels had a medium density in the wound area. Details on vessel density are shown in Figure 3. Smaller vessels were more prevalent at the WE, while medium or large diameter vessels were primarily observed in the WB.

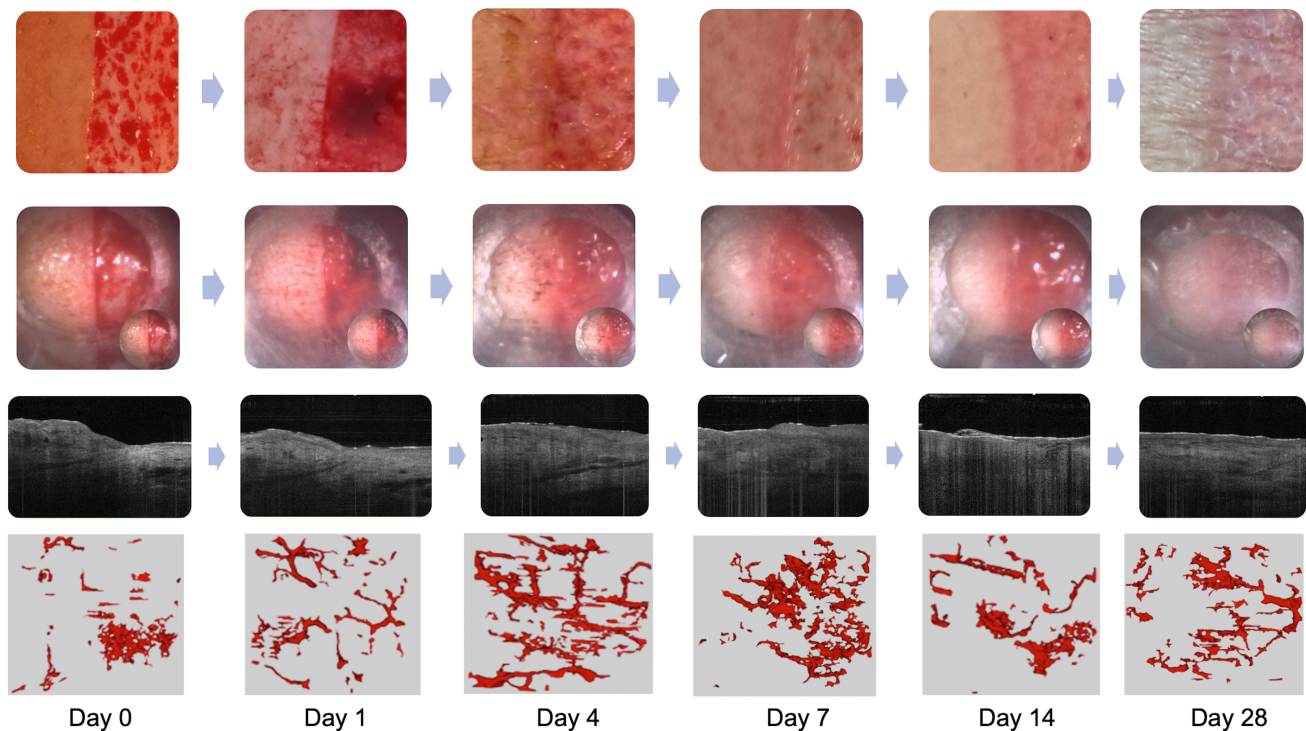


**FIGURE 4** Clinical pictures, clinical images in the OCT camera, cross-sectional OCT pictures and 3D images of the exact same position of wound healing over time. At the wound edge, numerous anastomosing high-density blood vessels were observed, especially between Days 1 and 7. In the wound bed, the vessels were frequently organized in a connecting pattern, whereas in healthy skin, the vessels appeared clustered with a small calibre.

### 3.2 | Vascular shapes in the vertical view depending on the measurement location (S12–14)

Spikes (WB and WE 100%, NSCL 66%) were more common than columns (WE 94%, WB 98%, NSCL 32%) (Table 2). Spikes and columns appeared significantly more often at WE and WB in comparison with NSCL (for all four  $p < 0.001$ ). Columns were significantly more present at WB in comparison with WE ( $p = 0.012$ ).

### 3.3 | Clinical and OCT cross-sectional features of wound healing over time

Clinically, after skin removal, punctiform bleedings occurred even on the day after surgery (Figure 4). On that day, serous exudate and a blot clot appeared and stayed until Day 7, typical of the proliferating phase of wound healing. From Day 7 to Day 28, crusts and a hyperaemic margin appeared. After 2 weeks, scar formation began, starting from the wound edge. In cross-sectional OCT images, the tissue loss could be observed as an uneven surface without a detectable epidermal layer. After 4 weeks, the cut was replaced by a continuous surface

with a lighter texture, corresponding to scar tissue. The epidermis and dermo-epidermal junction were again visible (Figure 4).

### 3.4 | Vascular shapes, branching and density over time (S2–14)

Figure 5 provides an overview of vessel shapes over time for WE, WB and NSCL. While the proportion of each vessel shape remained stable at 300 and 500  $\mu\text{m}$  depths, there was a decrease for some vessel shapes at 150  $\mu\text{m}$  depth. The details on wound healing dynamics for WE, WB and NSCL between the timepoints 0 and 28 (T0–T28) can be found in S2–S10. At 150  $\mu\text{m}$ , there were significant differences between T0 and T28 for blobs and serpiginous vessels at the WE. At 300  $\mu\text{m}$ , the number of serpiginous vessels at the WE, WB and NSCL was different between T0 and T28, as did the number of curved vessels in NSCL. At 500  $\mu\text{m}$ , the number of coiled vessels varied between Days 0 and 28 at the WE and WB. There were no significant differences between visits for spikes. However, for columns at WE, significant differences were visible between Days 4 and 7 and between Days 7 and 14.

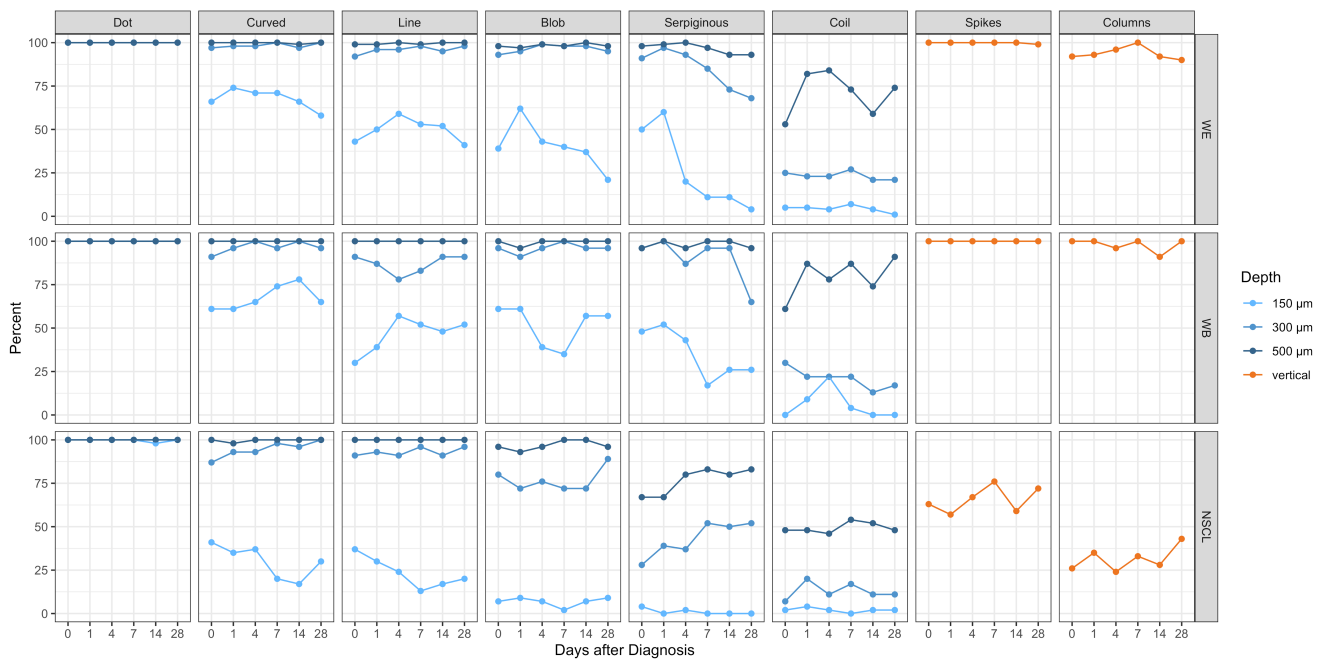


**FIGURE 5** An overview over vascular shapes over time for the wound edge (WE), wound bed (WB), normal skin 2 cm adjacent to the wounds and unaffected skin from the contralateral leg (NSCL).

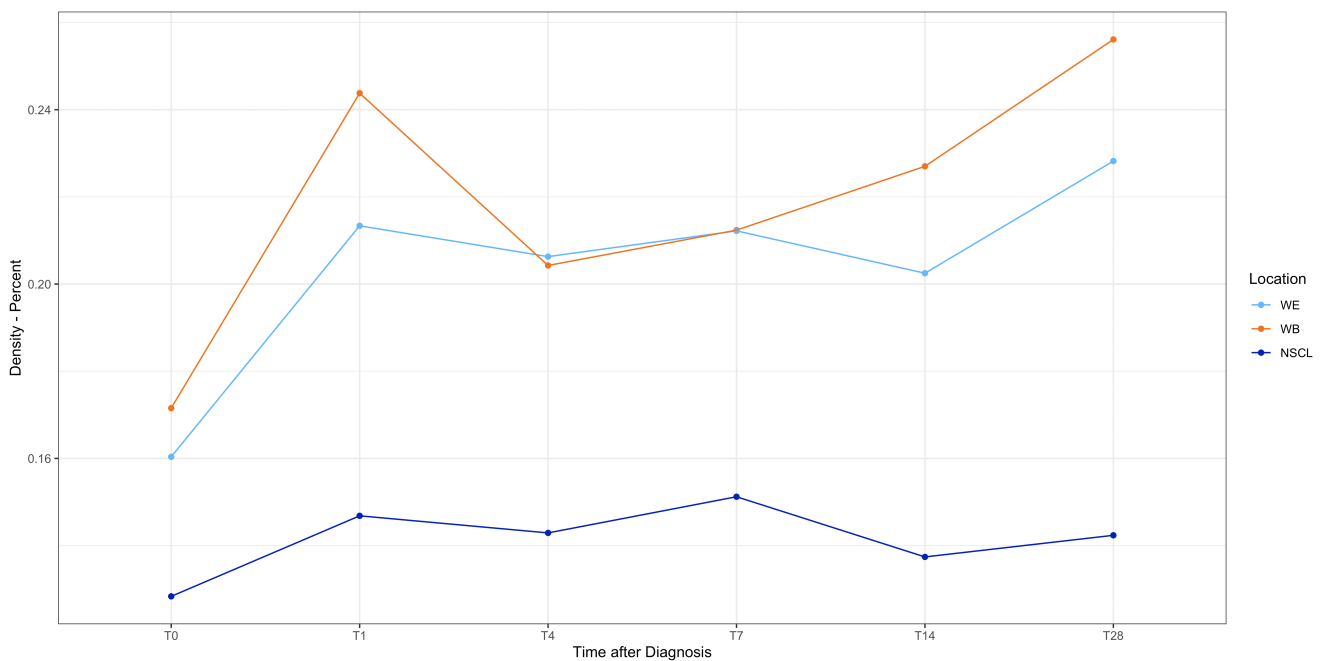


**FIGURE 6** An overview of overall vascular density time for the wound edge (WE), wound bed (WB), normal skin 2 cm adjacent to the wounds and unaffected skin from the contralateral leg (NSCL).

On the day of surgery, branched vessels were seen at WE. At both 150 and 300 μm depths, the number of branched vessels was highest on the first day and decreased from Day 4 to Day 28. At the WB, branched vessels decreased more slowly and remained the same from Day 7 to Day 28. At 150 μm, healthy skin showed

no branched vessels, but at 300 and 500 μm, they were present, although less than in the wound.

Figure 6 shows that healthy skin exhibited only low blood vessel density and no significant changes over time. Vessel density at WE and WB was significantly different between Day 0 and Day 28 ( $p < 0.001$ ). The first peak in



vessel density at WB and WE occurred on Day 1, followed by a decline over the next 4 days. Vessel density then increased again at both WE and WB, reaching its highest value on Day 28. All densities and *p*-values are presented in [S11](#).

## 4 | DISCUSSION

The purpose of this study was to examine split-thickness skin graft donor sides using D-OCT, to study the wound healing of acute superficial wounds. Monitoring acute wounds remains a challenge for current diagnostic devices. OCT is fast, easy to use and allows repeated non-invasive in vivo real-time imaging of the same site. Dynamic or angiographic OCT not only visualizes tissue morphology but also shows and quantifies blood vessels. The gold standard for wound follow-up is clinical assessment, which requires experience and is not objective, along with histology. However, histology is invasive and painful for the patient, causes injury to already damaged tissue and makes it difficult to monitor the same area as tissue is removed. Blood vessels collapse after biopsy, making it difficult to assess vessels in histology. Additionally, Doppler ultrasound can visualize large blood vessels, but the microcirculation, which is important for wound healing, is too small to be seen. Another disadvantage of ultrasound and confocal laser microscopy is that both require gel between the probe and the skin for imaging, posing a risk of infection. Nevertheless, the use of D-OCT in open wounds, even with sterile procedures, poses potential risks, particularly regarding infection and patient safety. Ethical considerations focus on ensuring that D-OCT does not increase the infection risk, necessitating strict sterile techniques, which can be challenging in high-throughput environments like emergency rooms compared with day hospitals or dedicated wound centres. Informed consent is essential, and the principle of “do no harm” must guide the use of D-OCT, considering alternative methods if risks are high. Maintaining sterility in emergency settings is difficult due to time and resource constraints, increasing cross-contamination risks. Mitigation steps include comprehensive staff training, using disposable equipment and considering alternative imaging methods when maintaining sterility is challenging. Ensuring patient safety through these measures is crucial to uphold ethical standards in clinical practice.

In our study, certain vessel types, such as serpiginous vessels, were significantly more common in the WB than at the edge. This could be because these vessels originate only from the deep dermal plexus and not from adjacent healthy skin. The same is true for blobs and coiled vessels, which may be responsible for attracting angioblasts

or endothelial cells.<sup>16</sup> Endothelial cells, in particular, form new capillaries, which could explain why larger vertical vessels, such as spikes and columns, emerge from the dermal plexus after injury and were found more frequently in the wound than in normal skin. Similar features were found after burn injuries, where large, so-called “truncated” vessels without branching were visible.<sup>17</sup>

Examining the morphology reveals that, after surgery, the incision caused chaos and breakage in the blood vessels. Later, a mesh network due to branching and higher vessel density was observed in the wound. Thus, angiogenesis of the few remaining capillaries could be initiated after injury, with branching and growth supporting the wound.<sup>18–20</sup> When wound healing processes like these are impeded, acute wounds can become chronic.<sup>21</sup> Our chronic wound study with D-OCT demonstrated different vessel morphology and density at the wound edges compared with healthy skin. Clusters of glomeruli-like vessels, clumps, greater blood perfusion and the absence of linear branching vessels were seen in the wound area of chronic venous ulcers.<sup>21,22</sup> The future of imaging wound healing will involve automated D-OCT monitoring, as described by Wang et al. in their study on diabetic wounds.<sup>23</sup>

3D images showed a section of vessels at the wound edge, typically with many small anastomosing vessels resembling ‘sprouting’.<sup>24,25</sup> Vessel density is higher in the wound than in healthy skin, as confirmed by other studies.<sup>25,26</sup> Surprisingly, in 3D images, the highest vessel density was found at the WB compared with the edge. This contrasts with the results of Tonnesen, while Gong et al. also demonstrated increased vessel density and diameter in acute burn wounds compared with contralateral healthy skin.<sup>2,27</sup> One reason for the lower vessel density at the wound edge might be that the entire tissue was examined, not just the edge. Another could be that crusts appearing earlier at the edge lead to poorer visualization of the vessels.<sup>28</sup> We were able to demonstrate that the vessel density at the exact wound edge, which is the original cut zone, was significantly higher than at the bed.

Wound healing in our study was comparable with other studies,<sup>18</sup> except that the rate of healing was slightly slower in some patients, possibly due to the older age of the participants. As age increases, the rate of cell division decreases, and molecular processes are altered.<sup>29–31</sup> As none of our patients were smokers, the results on wound healing were not impacted by smoking. Re-epithelialization was shown in vertical OCT images and might be faster at the wound edge due to the large number of mobilized keratinocytes from the lesion border compared with adnexal keratinocytes.<sup>32,33</sup> The time course results suggest that VEGF, which leads to

angiogenesis, may be responsible for the presence of ser-piginous vessels at 300  $\mu\text{m}$  for 7 days, coinciding with the exudative and resorptive phase of wound healing.<sup>34</sup>

Coils were mainly visible in the proliferation phase, but also in regeneration, which might be due to previous findings of coiled vessels in hyperplastic tissue.<sup>35</sup> Vessel density and branching increased significantly 1 day post-surgery and remained elevated, though less so, after weeks.<sup>36</sup> This increase might be attributed to high levels of VEGF, which directly correlate with a higher vessel density.<sup>34,37</sup> Wounds with complete re-epithelialization show reduced vessel density, indicating a potential indirect correlation between re-epithelialization and vessel density.

There are some drawbacks of our study due to intra- and inter-individual skin variations caused by differences in skin water content, age, sex and lesion localization.<sup>38,39</sup> Our study consisted of 23 split-thickness skin grafts from mainly elderly, non-smoking and Caucasian patients. Therefore, there are limitations related to sample size and demographic characteristics. The study's results may not be applicable to all age groups, genders or ethnicities, leading to biased findings. Future research should include larger and more diverse samples to ensure broader applicability, external validity and relevance of the results. Different dermatologists used the dermatome, so even with a fixed depth of 0.4 mm, the pressure on the skin could vary, resulting in different wound thicknesses of split-thickness skin grafts. Sawhney et al. demonstrated that wounds between 0.4 and 1.6 mm heal at the same rate. Therefore, deviations and the consequences for wound healing should be minimal.<sup>40</sup> Moreover, the dressing material and the frequency of change could impact wound healing. The use of polyurethane dressings, which were changed regularly in a standardized manner for all patients, leads to a higher number of blood vessels on the 7th and 10th postoperative days.<sup>41</sup> Another limitation is that D-OCT is technically unable to image beyond a depth of 0.5 mm, restricting the assessment to superficial layers, potentially missing critical data on deeper tissues involved in wound healing. This constraint can lead to incomplete evaluations, inaccurate diagnoses and inadequate monitoring of wound healing, affecting clinical decision-making and treatment outcomes. To overcome this, alternative methods such as high-frequency ultrasound (HFUS), magnetic resonance imaging (MRI) and photoacoustic imaging can be used. These technologies provide deeper tissue imaging and, when used in conjunction with D-OCT, offer a more comprehensive analysis, improving diagnosis, treatment planning and monitoring in clinical practice.

Another aspect to consider is that 4-week follow-ups often miss the full healing process in complex or chronic

wounds. Although this period may be sufficient for acute wounds, chronic wounds require longer-term studies with D-OCT, like those by Vélez et al., to gain comprehensive insights into long-term healing, recurrence patterns and treatment durability.<sup>22</sup> These extended studies enable thorough assessment, tracking the entire healing process, identifying recurrences and evaluating treatment durability over time. They should last several months to a year with regular D-OCT imaging, include diverse cases and provide quantitative metrics. Long-term studies improve diagnostic accuracy, detect early complications and refine treatment protocols for optimized care, demonstrating cost-effectiveness by reducing prolonged treatments and improving resource allocation. Extending studies beyond 4 weeks for chronic wounds is crucial for capturing the full benefits of D-OCT and improving patient outcomes.

## 5 | CONCLUSION

Conclusively, D-OCT allows repeated, non-invasive visualization of wound morphology, and the shape and density of superficial wound blood vessels in acute wounds over time. This method enables the monitoring of the exact same lesion, which cannot be achieved with a one-time invasive biopsy or other non-invasive devices that require gel for imaging, potentially leading to infection. Therefore, D-OCT may be useful in the future to detect wound healing disorders, study differences between acute and chronic wounds, and evaluate the effect of wound dressings. Future advancements in higher resolution, faster examination of larger surfaces and automatic software with artificial intelligence for vessel detection will enhance the applicability and provide more objective evaluations of wound healing in clinical practice.

## ACKNOWLEDGEMENTS

All authors fulfilled the criteria for authorship. The specific contributions to the study and manuscript of each of the authors were as follows: Sandra Schuh, Julia Welzel and Jon Holmes designed the research study and concept; Sandra Schuh and Maximilian Berger contributed essential D-OCT images for the study and acquired all the data; Sandra Schuh, Maximilian Berger and Julia Welzel planned the statistical analysis; Maximilian Berger, Sandra Schuh, Anna Rubeck and Stefan Schiele performed the statistical analysis, which was supervised by Sandra Schuh and Julia Welzel; Maximilian Berger analysed the D-OCT images, supervised by Sandra Schuh and Julia Welzel; Sandra Schuh wrote the paper; Maximilian Berger, Jennifer Jahel Vélez González, Julia Welzel and Jon Holmes critically revised the manuscript. All

authors have read and approved the final manuscript. They agreed to be accountable for all aspects of the work in ensuring that questions related to the accuracy or integrity of the work are appropriately investigated and resolved. Open Access funding enabled and organized by Projekt DEAL.

### FUNDING INFORMATION

The project is part of the ADVANCE (Automatic Detection of Vascular Networks for Cancer Evaluation) project, which received funding from the European Union's ICT Policy Support Program as part of the Competitiveness and Innovation Framework Program, Grant No. 621015. The manuscript reflects only the authors' views, and the European Union is not liable for any use that might be made of information contained herein.

### CONFLICT OF INTEREST STATEMENT

Julia Welzel and Sandra Schuh received a fee for the development of an OCT training platform from the Company DermoScan. Julia Welzel is the current President of the German Dermatological Society. Jon Holmes is CEO at Michelson Diagnostics and the manufacturer of the D-OCT used in this study. The other authors declare no conflicts of interests and declare that the manuscript contains original, unpublished work that is not being considered for publication elsewhere at this time.

### DATA AVAILABILITY STATEMENT

The data that support the findings of this study are available from the corresponding author upon reasonable request.

### ETHICS STATEMENT

The study was carried out with the ethics committee approval of the Ludwig-Maximilians University (Project Number 30-14) and the ethics vote of the University of Lübeck (No. 97-061) as a prospective, observational, non-interventional, longitudinal study. This study was guided according to the principles of the Declaration of Helsinki and international guidelines concerning clinical studies. They gave their written informed consent for publication of their case details.

### ORCID

Sandra Schuh  <https://orcid.org/0000-0002-1470-7619>

Maximilian Berger  <https://orcid.org/0009-0002-4649-3405>

Stefan Schiele  <https://orcid.org/0000-0003-2054-9052>

Anna Rubeck  <https://orcid.org/0009-0008-8730-7596>

Jennifer Jahel Vélez González  <https://orcid.org/0000-0003-2893-6188>

Jon Holmes  <https://orcid.org/0000-0001-9477-117X>

Julia Welzel  <https://orcid.org/0000-0002-6099-7418>

### REFERENCES

1. Neumaier M, Dorn-Beineke A, Blut. In: Scharl M, Gessler M, von Eckardstein A, eds. *Biochemie und Molekularbiologie des Menschen*. Urban Fischer Verlag; 2013:749-794.
2. Tonnesen MG, Feng X, Clark RA. Angiogenesis in wound healing. *J Invest Dermatol Symp Proc*. 2000;5:40-46.
3. Schuh S, Holmes J, Ulrich M, et al. Imaging blood vessel morphology in skin: dynamic optical coherence tomography as a novel potential diagnostic tool in dermatology. *Dermatol Ther (Heidelb)*. 2017;7:187-202.
4. Themstrup L, Welzel J, Ciardo S, et al. Validation of dynamic optical coherence tomography for non-invasive, in vivo microcirculation imaging of the skin. *Microvasc Res*. 2016;107:97-105.
5. Andersen PL, Olsen J, Friis KBE, et al. Vascular morphology in normal skin studied with dynamic optical coherence tomography. *Exp Dermatol*. 2018;27:966-972.
6. Mariampillai A, Standish BA, Moriyama EH, et al. Speckle variance detection of microvasculature using swept-source optical coherence tomography. *Opt Lett*. 2008;33:1530-1532.
7. Jonathan E, Enfield J, Leahy MJ. Correlation mapping method for generating microcirculation morphology from optical coherence tomography (OCT) intensity images. *J Biophotonics*. 2011;4:583-587.
8. An L, Qin J, Wang RK. Ultrahigh sensitive optical microangiography for in vivo imaging of microcirculations within human skin tissue beds. *Opt Exp*. 2010;18:8220-8228.
9. Zhao Y, Chen Z, Saxer C, et al. Doppler standard deviation imaging for clinical monitoring of in vivo human skin blood flow. *Opt Lett*. 2000;25:1358-1360.
10. Ren H, Ding Z, Zhao Y, Miao J, Nelson JS, Chen Z. Phase-resolved functional optical coherence tomography: simultaneous imaging of in situ tissue structure, blood flow velocity, standard deviation, birefringence, and stokes vectors in human skin. *Opt Lett*. 2002;27:1702-1704.
11. Boas DA, Dunn AK. Laser speckle contrast imaging in biomedical optics. *J Biomed Opt*. 2010;15:011109.
12. Manfredi M, Grana C, Pellacani G. Skin surface reconstruction and 3D vessels segmentation in speckle variance optical coherence tomography. In: proceedings of the 11th joint conference on computer vision, imaging and computer graphics theory and applications (VISIGRAPP). *Scitepress Rome*. 2016;4:234-240.
13. Ulrich M, Themstrup L, de Carvalho N, et al. Dynamic optical coherence tomography of skin blood vessels – proposed terminology and practical guidelines. *J Eur Acad Dermatol Venereol*. 2018;32:152-155.
14. Themstrup L, De Carvalho N, Nielsen SM, et al. In vivo differentiation of common basal cell carcinoma subtypes by microvascular and structural imaging using dynamic optical coherence tomography. *Exp Dermatol*. 2018;27:156-165.
15. Themstrup L, Ciardo S, Manfredi M, et al. In vivo, morphological vascular changes induced by topical brimonidine studied by dynamic optical coherence tomography. *J Eur Acad Dermatol Venereol*. 2016;30:974-979.

16. Demidova-Rice TN, Durham JT, Herman IM. Wound healing angiogenesis: innovations and challenges in acute and chronic wound healing. *Adv Wound Care*. 2012;1:17-22.
17. Lindert J, Taffazoli-Lari K, Tüshaus L, et al. Optical coherence tomography provides an optical biopsy of burn wounds in children – a pilot study. *J Biomed Opt*. 2018;23:1-6.
18. DiPietro LA. Angiogenesis and scar formation in healing wounds. *Curr Opin Rheumatol*. 2013;25:87-91.
19. DiPietro LA. Angiogenesis and wound repair: when enough is enough. *J Leukoc Biol*. 2016;100:979-984.
20. Greaves NS, Ashcroft KJ, Baguneid M, Bayat A. Current understanding of molecular and cellular mechanisms in fibroplasia and angiogenesis during acute wound healing. *J Dermatol Sci*. 2013;72:206-217.
21. Holmes J, Schuh S, Bowling FL, Mani R, Welzel J. Dynamic optical coherence tomography is a new technique for imaging skin around lower extremity wounds. *Int J Low Extrem Wounds*. 2019;18:65-74.
22. Vélez González JJ, Berger M, Schiele S, et al. Dynamic optical coherence tomography of chronic venous ulcers. *J Eur Acad Dermatol Venereol*. 2023;38:223-231. doi:10.1111/jdv.19496
23. Wang Y, Freeman A, Ajjan R, del Galdo F, Tiganescu A. Automated quantification of 3D wound morphology by machine learning and optical coherence tomography in type 2 diabetes. *Skin Health Dis*. 2022;3:e203.
24. Eming SA, Martin P, Tomic-Canic M. Wound repair and regeneration: mechanisms, signaling, and translation. *Sci Transl Med*. 2014;6:265sr6.
25. Li J, Chen J, Kirsner R. Pathophysiology of acute wound healing. *Clin Dermatol*. 2007;25:9-18.
26. Diegelmann RF, Evans MC. Wound healing: an overview of acute, fibrotic and delayed healing. *Front Biosci*. 2004;9:283-289.
27. Gong P, Eshaghian S, Wood FM, et al. Optical coherence tomography angiography for longitudinal monitoring of vascular changes in human cutaneous burns. *Exp Dermatol*. 2016;25:722-724.
28. Stavrou D. Neovascularisation in wound healing. *J Wound Care*. 2008;17:298-300.
29. Gilchrist BA. In vitro assessment of keratinocyte aging. *J Invest Dermatol*. 1983;81:184s-189s.
30. Swift ME, Burns AL, Gray KL, DiPietro LA. Age-related alterations in the inflammatory response to dermal injury. *J Invest Dermatol*. 2001;117:1027-1035.
31. Gould L, Abadir P, Brem H, et al. Chronic wound repair and healing in older adults: current status and future research. *J Am Geriatr Soc*. 2015;63:427-438.
32. Duckney P, Wong HK, Serrano J, Yaradou D, Oddos T, Stamatias GN. The role of skin barrier in modulating the effects of common skin microbial species on the inflammation, differentiation and proliferation status of epidermal keratinocytes. *BMC Res Notes*. 2013;6:474.
33. Marschall S, Sander B, Mogensen M, Jørgensen TM, Andersen PE. Optical coherence tomography – current technology and applications in clinical and biomedical research. *Anal Bioanal Chem*. 2011;400:2699-2720.
34. de Mendonça RJ. Angiogenesis in wound healing. In: Davies J, ed. *Tissue Regeneration – from Basic Biology to Clinical Application*. InTech; 2012:93-108.
35. Ryan TJ. Pathophysiology of skin capillaries. *Int J Dermatol*. 1975;14:708-721.
36. Flegg JA, Menon SN, Maini PK, McElwain DLS. On the mathematical modeling of wound healing angiogenesis in skin as a reaction-transport process. *Front Physiol*. 2015;6:262.
37. Johnson KE, Wilgus TA. Vascular endothelial growth factor and angiogenesis in the regulation of cutaneous wound repair. *Adv Wound Care*. 2014;3:647-661.
38. Akdeniz M, Tomova-Simitchieva T, Dobos G, Blume-Peytavi U, Kottner J. Does dietary fluid intake affect skin hydration in healthy humans? A systematic literature review. *Skin Res Technol*. 2018;24:459-465.
39. Mehta HH, Nikam VV, Jaiswal CR, Mehta HB. A cross-sectional study of variations in the biophysical parameters of skin among healthy volunteers. *Indian J Dermatol Venereol Leprol*. 2018;84:521.
40. Sawhney CP, Subbaraju GV, Chakravarti RN. Healing of donor sites of split skin grafts. An experimental study in pigs. *Br J Plast Surg*. 1969;22:359-364.
41. Loeffelbein DJ, Rohleder NH, Eddicks M, et al. Evaluation of human amniotic membrane as a wound dressing for split-thickness skin-graft donor sites. *Biomed Res Int*. 2014;2014:572183.

## SUPPORTING INFORMATION

Additional supporting information can be found online in the Supporting Information section at the end of this article.

**How to cite this article:** Schuh S, Berger M, Schiele S, et al. Dynamic optical coherence tomography for imaging acute wound healing. *Int Wound J*. 2024;21(8):e70015. doi:10.1111/iwj.70015